Chapter 4

Synthesis of ZnS Nanoparticles using *thiol* as Template, Their characterization and Application as Photocatalyst

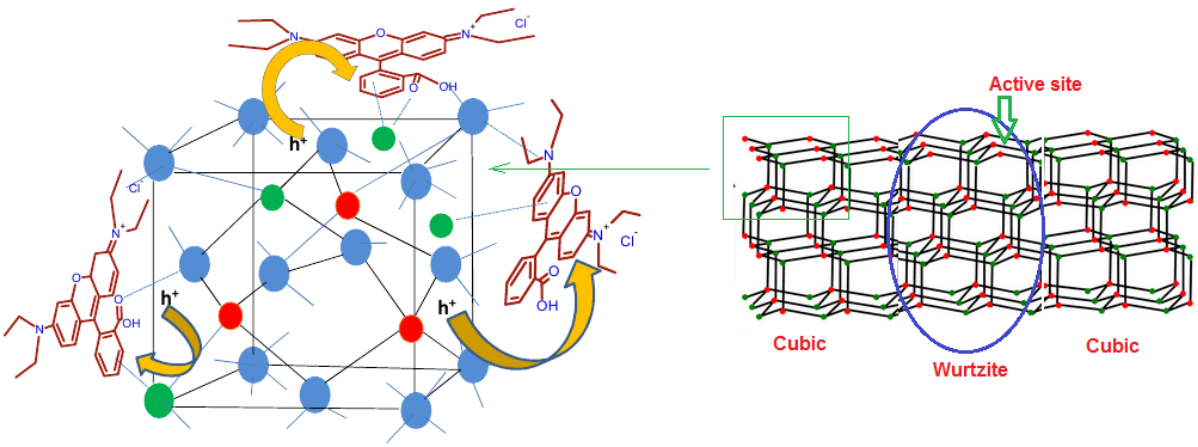

We have demonstrated that on doping the type of semiconductor can be changed and also phase change can be induced which directly affect the photocatalytic activity of the material.

Communicated

4.1 Introduction

Industrialization is one of the markers of progress for any country. Although it generates employment and other opportunities, nevertheless, it also poses plenty of problems related to natural resources that need to be tackled. Water pollution is one of such problems as many industries dump its effluent into the natural water bodies. These harm the environment and aquatic lives.

Figure 4.1.Acuteness of water pollution problem.

Various physical, chemical, and biological methods are available to treat polluted water before being released outside. Physical methods (like absorption, adsorption, membrane technologies) and chemical methods (like coagulation, flocculation) have limitations in that these can only concentrate and settle the waste.

Figure 4.2.Water treatment plant.

On the other hand, biological methods (using a specific bacterial culture) demand extra care and special conditions, besides cost. Destructive techniques such as incineration of the concentrated waste or chemical oxidation lead to additional problem of air pollution (Figure 4.3).

Figure 4.3. Plant showing incinerator one of the causes for air pollution.

The type of treatment adopted by an industry depends on many factors such as its size, production rate, public or private sector involvement and last but not the least profit consideration. Many innovative and low-cost techniques are proposed and implemented nowadays to tackle such problems.

Photocatalysis by semiconducting material is one of techniques to abate water pollution.[1]Besides being effective and low-cost, it also offers almost complete mineralization of the pollutants. When exposed to a light of suitable wavelength, it absorbs energy sufficient to excite electrons in HOMO of the valence band (VB) to LUMO of the conductance band (CB) and generate electron-hole pairs in the respective bands (Figure 4.4 and 4.5).

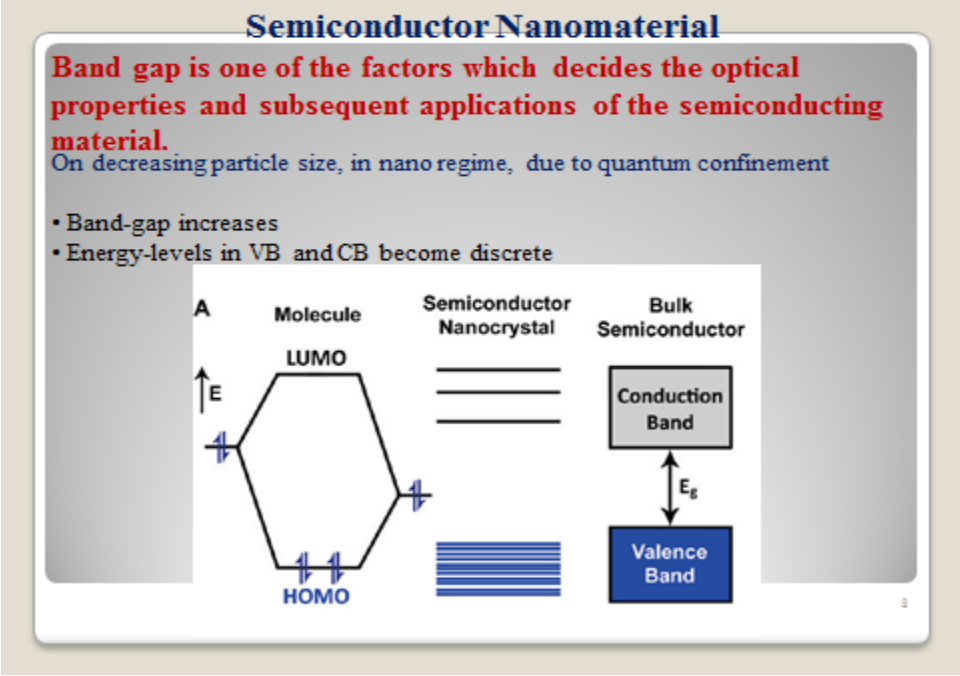

Figure 4.4. Energy levels and band gap of the bulk semiconductor and semiconductor nanoparticles.

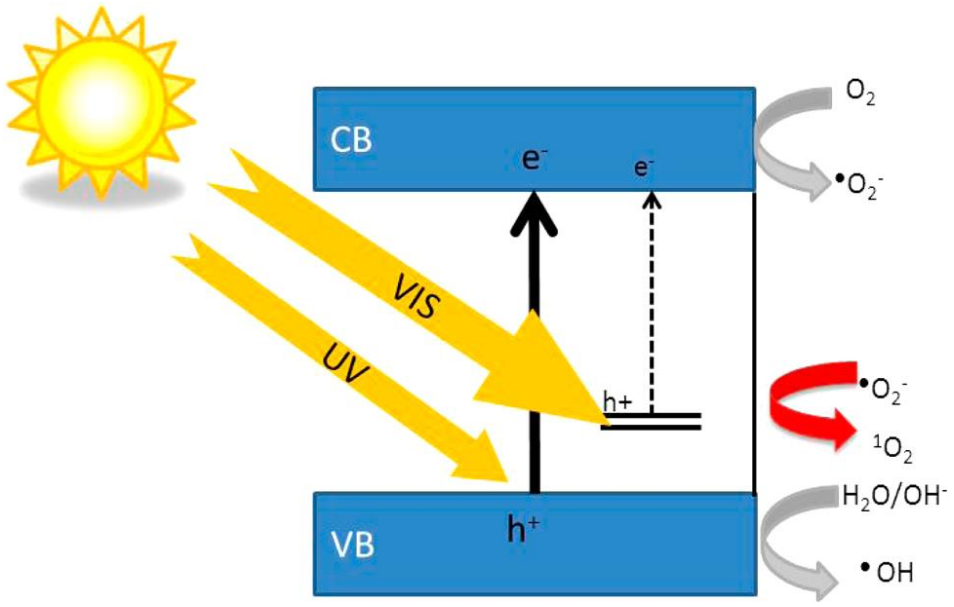

Figure 4.5.Schematic of semiconductor photocatalysis (Fisher, M. B.; Keane, D. A.; Fernández-Ibáñez, P.; Colreavy, J.; Hinder, S. J.; McGuigan, K. G.; Pillai, S. C. Appl. Catal., B 2013, 130−131, 8−13).

These charge carriers have a natural tendency to recombine either in a radiative or in a non-radiative manner. The photocatalytic efficiency of the material depends on the longevity of these charge carriers and the dynamics of these charge carriers is governed by thermodynamic and kinetic parameters. For example, defects due to anion or cation vacancies (lattice defects), impurities present at interstitial sites, shallow and deep surface states, etc., play an important role in trapping the charge carriers before recombination, in turn, extending their longevity.[2]These isolated electrons and holes have a thermodynamic tendency to diffuse toward the surface and initiate redox processes.[3] Amongst these charge carriers on the surface,

electrons are easily available to the adsorbed molecules (pollutants or dissolved oxygen present in water) leading to generation of free radicals – a reactive species which can initiate a sequence of secondary chain reactions. On the other hand, the holes present on the surface oxidize the adsorbed molecules and generate cationic species, also, capable to initiate a sequence of secondary chain reactions (Figure 4.6).

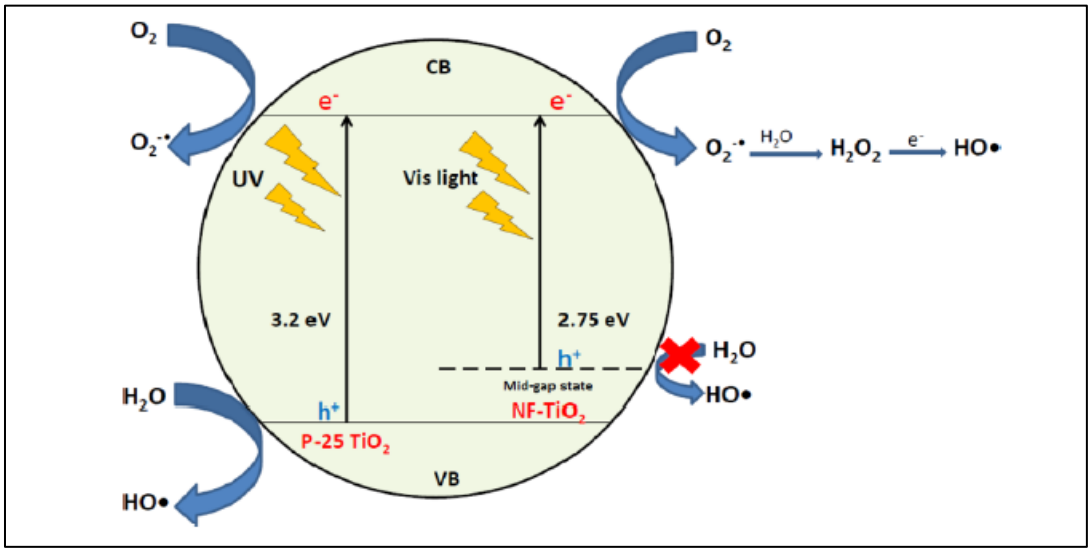

Figure 4.6. Production of different ROS during the visible-light-active photocatalytic processes for the destruction of 6-hydroxymethyl uracil (Zhao, C.; Pelaez, M.; Dionysiou, D. D.; Pillai, S. C.; Byrne, J. A.; O'Shea, K. E. Catal. Today 2014, **70**,224**).**

Another parameter, which controls the photocatalytic efficiency, is the band-gap between valence band (VB) and conductance band (CB) of the semiconducting material. The band-gap can be tailored according to end-applications by different methods.[4] For example; it can be increased by decreasing the particle size of the material and, at nano domain, becomes definite and discrete.[5, 6] The band-gap can

be decreased by introducing suitable dopant ions, particularly from transition metal or lanthanide group. Judiciously selected dopant ions add extra energy levels between the VB and the CB of the host.[7, 8]The physical properties of the semiconducting material can be tuned by reducing the particle size along with appropriate doping. Many research groups are engaged in improving the photcatalytic performance of semiconducting materials; for instance, Schneider's group recently developed Cu-doped ZnS quantum dots and coupled it with anatase TiO_2 nanoparticles to form TiO_2/Cu:ZnS nanocomposite. They observed an enhanced photocatalytic performance compared to either pure TiO_2 or undoped TiO_2/ZnS nanocomposite.[9]Recently, S. Li. et al. synthesized CdS nanowires and generated shallow surface states by light Ni^{2+} doping. Using Surface Photovoltage Spectroscopy (SPV), Transient Photovoltage (TPV) measurements and photoluminescence (PL) spectroscopy, they demonstrated that these shallow and deep surface states make the photogenerated charge carriers separate, leading to the enhanced photocatalytic efficacy of the material.[10] It was observed that photocatalytic performance of the semiconducting material is boosted in presence of co-catalyst,[11] by entrapping the material in polymeric film[12] etc.

Zinc Sulphide (ZnS) is a semiconducting material from II-VI class.It finds application in phosphor, light emitting diode (LED), sensor and laser.[13, 14]It has a band-gap of 3.5-3.7 eV and 3.7-3.8 eV for sphalerite and wurtzite phase

respectively.[15]Advantage of using ZnS semiconductor is that it can be synthesized easily by simple wet chemical method and at nano level, its particle size, surface and other physical properties canbe easily controlled using capping ligands like polyvinylpyrrolidine (PVP), mercaptopropanoic acid, acrylic acid, methacrylic acid, etc.[16, 17]Pouretedal et al. reported ZnS nanoparticles (NPs) doped with Mn^{2+},Ni^{2+}, and Cu^{2+} as nano-photocatalyst for the degradation of colored pollutants.[18]They showed that transition metal ions (dopants) enhance the efficiency of the photocatalyst. Bang et al. reported hexagonal Ni^{2+} doped ZnS NPs as promising photocatalyst.[19]Chen et al. reported the solvo-thermal synthesis of well-dispersed ZnS nanorods with efficient photocatalytic properties.[20]

In this study, our strategy is first to modify and control the band gap in ZnS semiconductor by reducing the particle size to nano level (quantum dots) making it possible to generate electrons and holes (charge carriers) as separate as possible. Secondly, the separated charge carriers can be trapped at pre-constructed shallow and deep surface states that are produced by dopant Ni^{2+} ions. The photocatalytic activity of the synthesized NPs has been evaluated using aqueous solution of RhB, as a prototype dye, under uv-vis radiation from HPMV lamp.

4.1 Experimental

4.1.1 Material

Analytical grade zinc acetate dihydrate (Zn $(CH_3COO)_2 \cdot 2H_2O$), nickel acetate dihydrate (Ni $(CH_3COO)_2 \cdot 2H_2O$), Sodium sulfide $Na_2S.xH_2O$,Rhodamine B (RhB), terpthalic acid (S. D. Fine Chemicals Ltd., India), 2-Mercaptoethanol ($HSCH_2CH_2OH$),sodium hydroxide (NaOH) - LobaChemie, India were used without further purification.

4.1.2 Method

In our previous study, we had reported the synthesis of ZnS NPs with different weight percent of Ni doping.[21]Briefly it can be described as: solutions of Zinc acetate (0.025mol dissolved in 25 mL methanol) and nickelacetate (1.386×10^{-3}mol dissolved in 25 mL methanol for 5%) were mixed under continuous stirring followed by addition of mercaptoethanol (0.025 mol). The pH of the mixture was maintained to 10.2 using an aqueous solution of NaOH (1 M) throughout the reaction.Then, the temperature of the reaction mixture was raised to 70 ^oC and aqueous solution of sodium sulfide (25 mL, 0.025 mol) was injected immediately. The reaction mixture was continuously stirred for 3h to form a homogenous stabilized dispersion at the same temperature. After 3h, the mixture was cooled and centrifuged at 8000 rpm. The precipitates were washed with deionised water

several times and then dried at 100^{o}C to obtain a ZnS:Ni^{2+} powder sample. Other samples of ZnS NPs with different dopant concentration were prepared by taking nickel acetate concentration 2.778 x 10^{-3}mol (for 10.0%). Similarly, pristine (without dopant) sample of ZnS NPs was also synthesized.

Photocatalytic efficiency of the synthesized material was evaluated under uv-vis light from 250 W HPMV lamp.[22]The lamp was placed inside the double wall glass tube surrounded by circulating cold-water. The whole assembly was kept in another glass cylinder of the photo-reactor containing reactants and magnetic needle. Subsequently, 400 mL of aqueous solution of RhB (10^{-4} M, 47.902 ppm) was mixed with 5 mg synthesized NPs at RT, pH 6.5 and thoroughly mixed in dark for 60 min. Subsequently; the mixture was transferred to the photo-reactor (Figure 4.7). At every 10 min, the sampling (5 mL) of the irradiated solution was carried out up to 180 min. Then, the solution in photo-reactor was centrifuged at 10,000 rpm to remove the catalyst. The concentration of RhB present in the solution was determined spectrophotometrically.

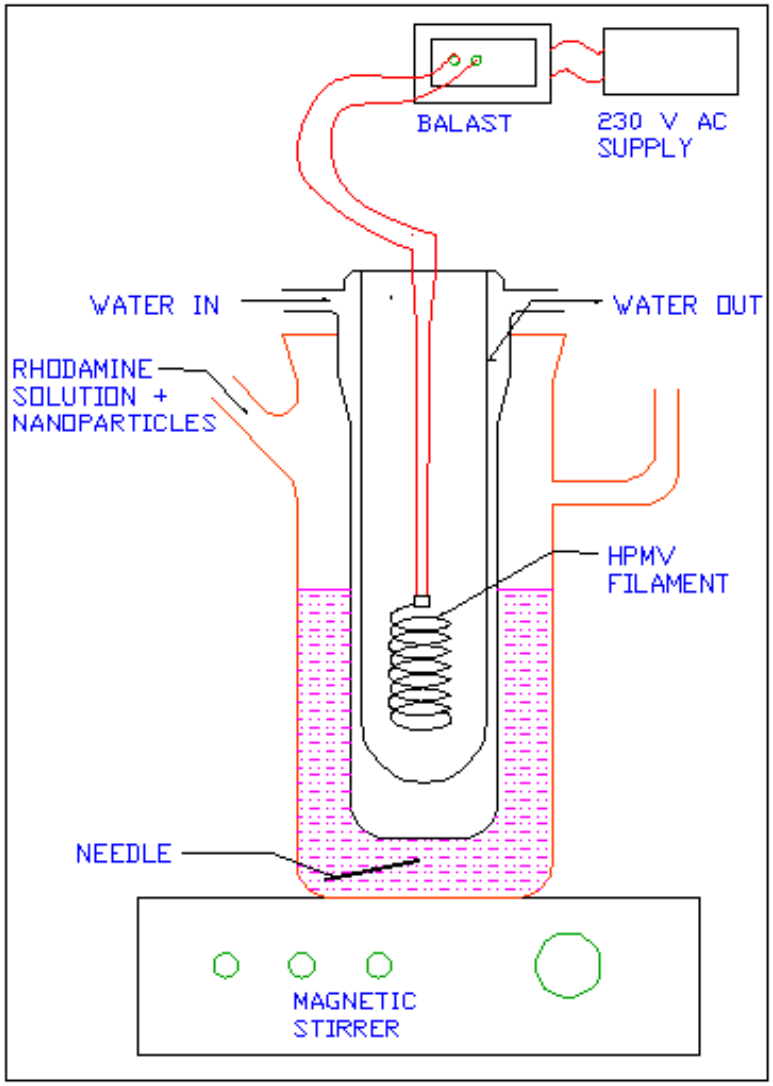

Figure 4.7. Design of photochemical reactor used for this study to degrade RhB solution in presence of synthesized photocatalyst.

4.1.3 Characterization

The X-ray powder diffraction (XRD) analysis of the samples was carried out by using a Guinier X-ray powder diffractometer (Bruker D8) with Cu Kα radiation, λ=0.15418 nm. Particle size was determined by TEM (Philips Tecnai 20). The compositional analysis of the powder samples was carried out by using Inductive

Coupled Plasma-Atomic Emission spectroscopy (ICP-AES) analysis (Perkin-Elmer Optima 3300 RL).The solid sample was dispersed in water, sonicated for 10 min to record UV-Vis absorption spectra on a Perkin Elmer Lambda 35 UV-Vis spectrometer. PL spectra were recorded on a Jasco FP-6300 spectrophotometer using Xenon lamp as an excitation source at 280 nm. All measurements were made at 25^{o}C in deionized water. The MS and CV studies were performed using Electrochemical Analyzer (CHI600E, CH instruments, Inc., Austin, TX). The semiconductor electrode on ITO glass was used as a working electrode. Before making a layer of ZnS NPs (pristine as well as doped), the ITO glass was degreased for 10 min using a surfactant solution, followed by rinsing with distilled water and alcohol for 15 min in an ultrasonic bath. The ZnS NPs (pristine or with dopant) were suspended in an organic polar solvent (ethanol: DMSO, 1:0.2) and the resultant solution was spin-coated on clean substrates at 3000 rpm for 60 sec, and the spin-coated film was then kept in an oven at 50˚C for 20 min. A saturated calomel electrode (SCE for CV and MS) was used as reference and platinum wire was used as a counter electrode.The aqueous solution of KCl (0.1 M) was used as a supporting electrolyte. The cyclic voltammetry was carried out at 25 mV/ s scan-rate. The type (n/p type) of the semiconducting material was determined by the hot-probe method.

4.3 Results and discussion

The X-ray diffraction patterns of the synthesized ZnS and ZnS:Ni^{2+} NPs are shown in Figure 4. 2. The XRD peaks are broad as compared to bulk ZnS due to the nano regime.[23] Three major peaks at 2θ values of 29.06, 48.37, and 57.42^{o} correspond to (111), (220), and (311) planes, respectively. It has been observed that out of these three main features, the peaks corresponding to (311) merged in background.The XRD patterns for pristine and 5% ZnS NPs samples are well-matched with the standard cubic ZnS (for pristine and 5% Ni^{2+} doped, JCPDS card No. 79-0043). At 10% concentration of Ni^{+2}, the broad peak corresponded to (111) planes in cubic phase, became distorted and (101) shoulder became more intense along with the (002) and (100) peaks. This distortion of peaks clearly indicates that phase changes from cubic sphalerite to hexagonal wurtzite (JCPDS card No. 79-2204 for 10% Ni^{+2}).On the basis of the Full Width at Half Maximum (FWHM) of major XRD peak (111) and the Debeye-Scherrer formula,[24]the average crystallite size was calculated and in the range of 4-5 nm. Further, the XRD pattern reveals that the pristine ZnS NPs are amorphous in nature. On the other hand, on increasing the amount of dopant, the crystallinity increases. At 10% Ni^{2+} concentration, the pattern is distinct and manifests the cubic phase. This behavior can be explained in terms of the readjustment of lattice structure to minimize the potential energy. As the size of Ni^{2+} (72 pm) and Zn^{2+} (74 pm) is almost similar, on doping, Ni^{2+} ions

may fill the vacant Zn^{2+} sites and thereby decrease the substitutional lattice defects.[25]

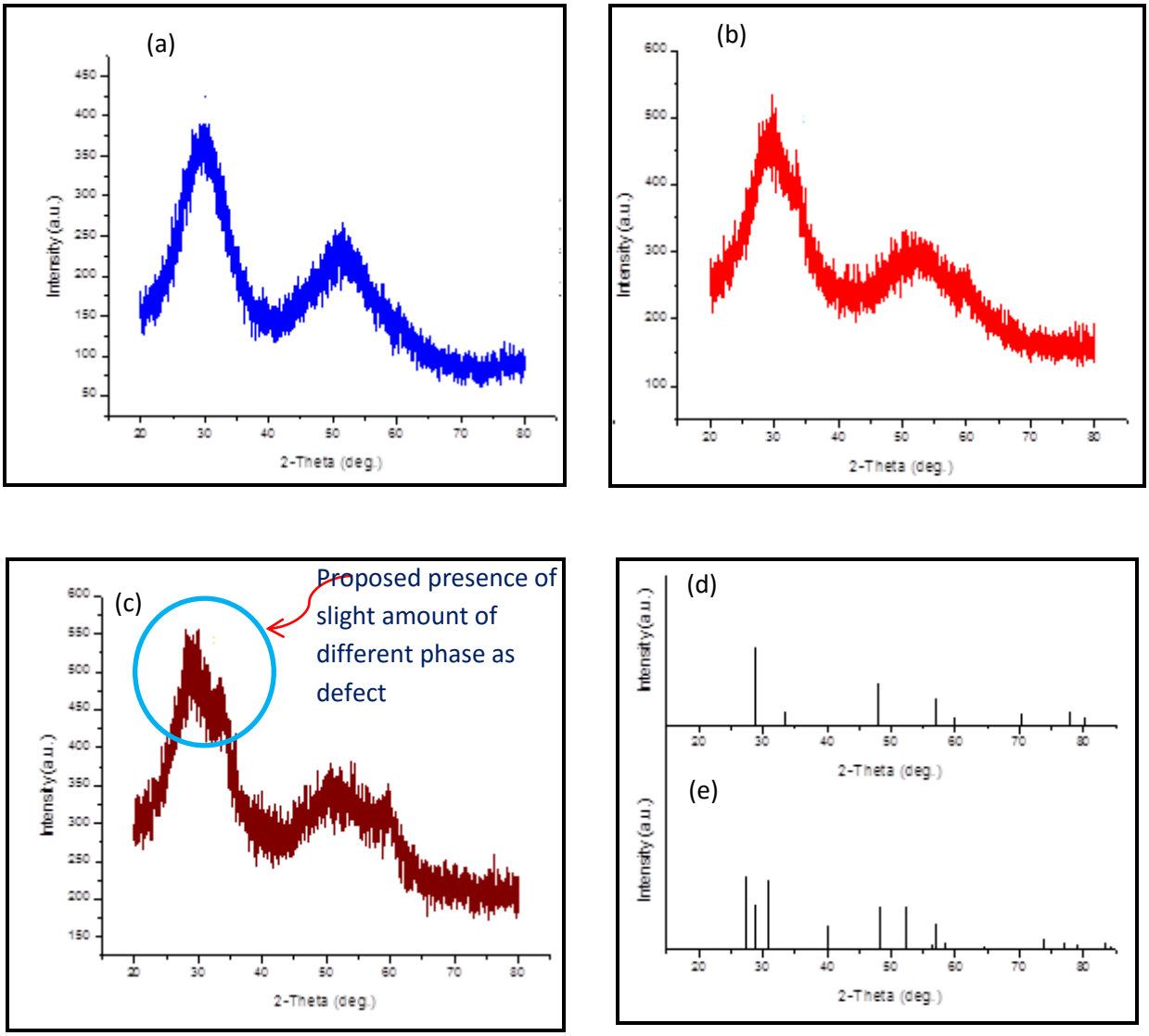

Figure 4.8 XRD pattern of ZnS NPs. (a) pristine (b) 5.0 % (c) 10.0% Ni as dopant ions (d) standard cubic ZnS pattern as per(JCPDS card No. 79-0043) and (e) standard wurtzite ZnS as per (JCPDS card No. 79-2204).

The amount of dopant ions in the samples are analyzed using ICP-AES analysis shown in Table 4.S1. The morphology of the nanoparticles is studied by using

TEM analysis (Figure 4.3). The ZnS NPs (both pristine and doped with 10% Ni) are almost spherical having a size in the range of 80 -120 nm. The inset of the Figure 4.S1 (SAED pattern) supports the observation from XRD that the sample having 10% dopant is more crystalline than the pristine ZnS NPs.

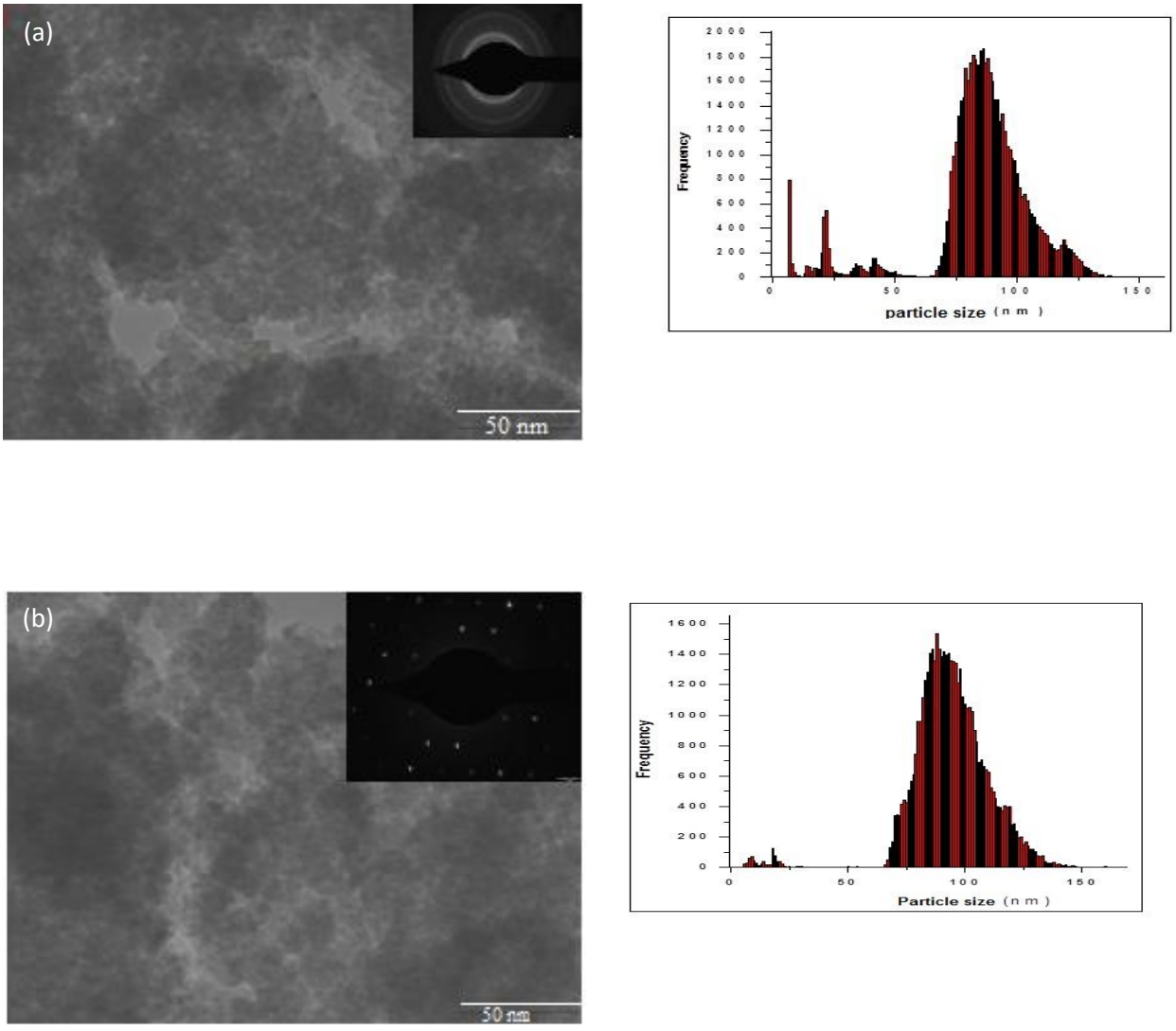

Figure 4.9.TEM images with particle size histogram of (a) pristine and (b) doped ZnS:Ni (10 %) NPs (insets shows the SAED pattern).

The UV absorption spectra (200 to 400 nm) of pristine and ZnS: Ni^{2+} samples in aqueous solution are shown in Figure 4.4. The absorption spectrum of pristine ZnS NPs reveals a sharp onset followed by sharp edge indicates the narrow particle size distribution. The absorption edge displays a blue shift (270 nm) compare to the bulk ZnS (335 nm) due to quantum confinement effect [26]indicates broadening of the band gap and discreteness of the bands. This increases the longevity of charge carriers at room temperature resulting in sharp band-edge transition in the UV region. All spectra show absorption maxima on an average at 270 nm. Dustan et al. explained these bands due to excess Zn^{2+} ions.[27]It can be seen that on increasing the amount of Ni^{2+} ions the intensity of absorption at 270 nm increases (up to 5%). This is due to the band-to-band electronic transitions. However, at 10% dopant concentration, the intensity of the same is reduced due to crystallinity of the material.[25]At 10% dopant level, the Ni^{2+} ions not only provide extra energy levels but also fulfill the lattice defect sites. This leads to an increase in crystallinity whereby the host's energy levels become discrete resulting into a decrease in band-to-band transition in this region. XRD results also support this argument.

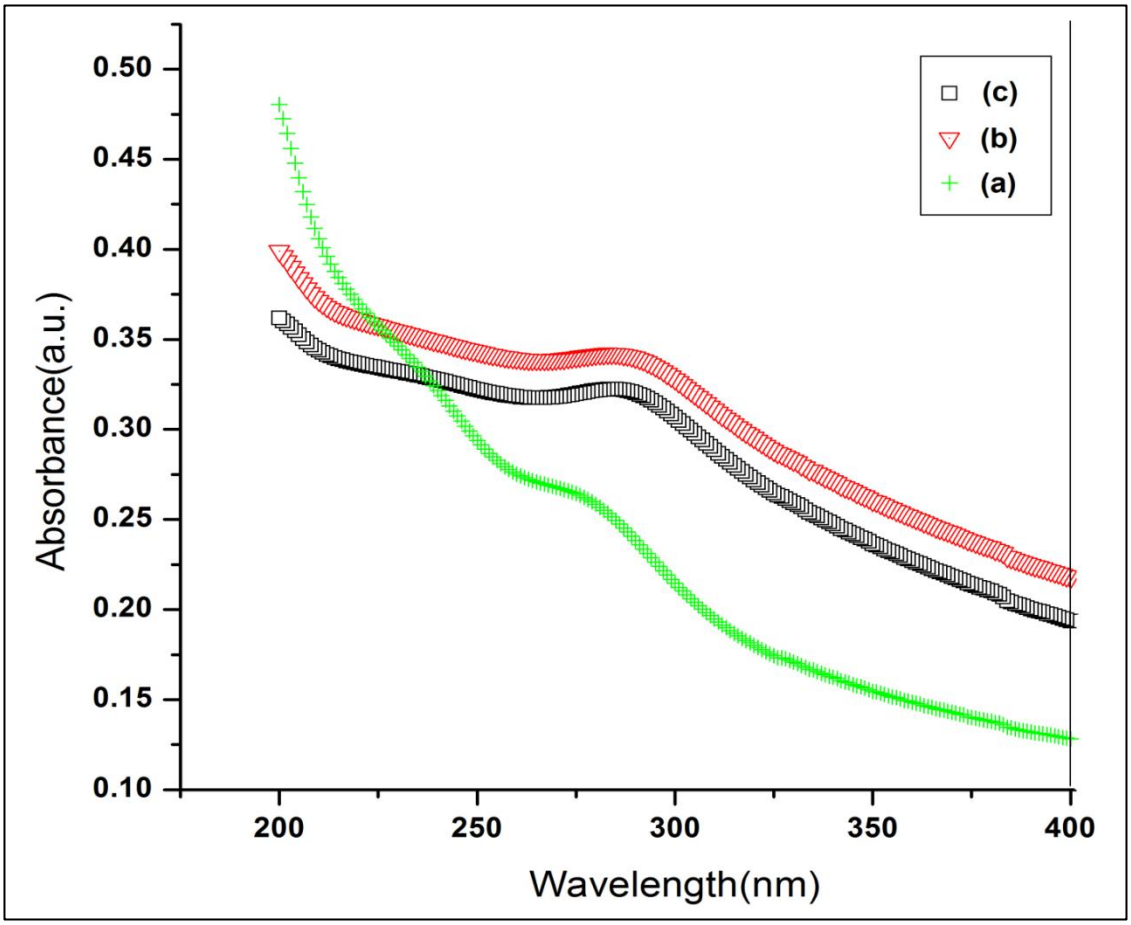

Figure 4.10. UV absorption spectra of (a) ZnS undoped (b) ZnS:Ni^{2+}(5.0%) and (c) ZnS:Ni^{2+}(10.0%).

The band gap was calculated using the modified Kubelka-Munk function. The direct band gap energy was obtained from a plot of $(\alpha h\nu)^2$vs photon energy (hν)using the relationship[28]

$$(\alpha h\nu)^2 = A(h\nu - E_g) \qquad (1)$$

where, hν is the photon energy, α, the absorption co-efficient (α=4πk/λ, k is absorbance, λ is wavelength in nm), E_g, the band gap energy, and A, a constant. The value of direct band gap energy was determined by extrapolating the straight-line portion of the curve to the hν-axis (Table 4.S1). Direct band gap increases

from 3.68 eV (bulk) to 4.43 eV (pristine NPs) and then decreases to 4.29 eV on doping Ni^{2+} ions. The decrease in the band gap on doping indicates that Ni^{2+} ions provide extra energy levels between VB and CB of host.[29] Figure 5 shows the PL spectra of synthesized NPs with excitation wavelength of 280 nm. The PL spectrum shows two predominant peaks, one in the violet region at 330 nm and the other in the blue region at 425 nm. In case of pristine ZnS NPs, the peak at 330 nm has high intensity due to radiative recombination processes between electrons (in CB) and holes (in VB). The peak at 425 nm is due to defect sites (absence of Zn^{2+} or S^{2-} ions in ZnS lattice sites)and radiative transition of electrons from shallow trap states (ST) near the CB to sulfur vacancies (V_s) near the VB.[30]On doping ZnS with 5% Ni^{2+}, the intensity of PL peak at 330 nm increases while at 425 nm decreases.This observation indicates that doping of the impurity ions produces more defects and provides the extra energy levels between VB and CB.This results into faster radiative recombination processes.[21]The almost quenching of the peak at 425 nm with 10% dopant concentration indicates trapping of electrons in ST leaving free holes in the VB.[31]The charge carriers trapped into such defects decrease their recombination rate and enhance longevity. Generally, this situation is favorable for photocatalysis. Due to separation of electrons and holes for a longer time have a thermodynamic tendency to diffuse towards the surface, which can further be exploited for photocatalytic reactions.[32]Hence, from this study it is

established that tuning between crystallinity and defects is possible by varying the amount of dopant. Optimum performance in term of photocatalytic activity can be achieved by controlling the amount of impurity in the host material.

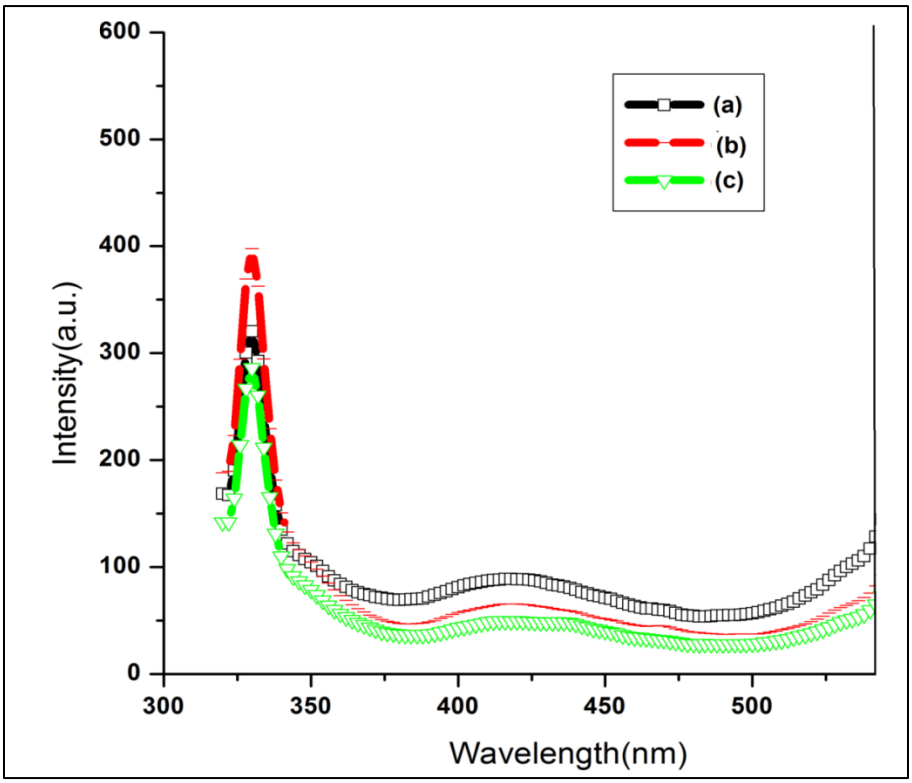

Figure 4.11. Photoluminescence spectra of ZnS NPs samples: (a) ZnS undoped (b) ZnS:Ni^{2+}(5.0%) and (c) ZnS:Ni^{2+}(10.0%).

4.4 Photocatalytic performance of pristine ZnS and Ni doped ZnS NPs.

Photocatalytic activity of synthesized NPs was evaluated spectrophotometrically in term of change in absorption intensity (λ_{max} at 555 nm) of RhB in aqueous solution. The % decolorization efficiency of samples was calculated as

$$\%\, Efficiency = 100 \times \frac{[Ao - A]}{Ao} = 100 \times \frac{[Co - C]}{Co} \qquad (2)$$

where, A_o, A, C_o, and C are initial absorbance, absorption after irradiation at various time intervals, initial concentration of solution, and concentration of dye after irradiation at various time intervals, respectively. Pure RhB dissolved in water shows negligible degradation (due to the presence of •OH free radical generated from water) in 180 min when irradiated under uv-vis light. Figure 4.12 shows the time-dependent uv-vis absorption spectra of RhB during photo irradiation in presence of synthesized ZnS NPs at every 10 min time interval and Figure 4.13 compares the degradation efficiency of the same (see Figures 4.S1 and 4.S2). The decrease in intensity of λ_{max} at 555 nm indicates the degradation of the dye under experimental conditions. It is observed (Figure 4.12a) that pristine ZnS NPs degrade RhB slowly within the given period (upto 120 min) and at the end of 120 min, it degrades almost 65% of the dye. The 5% Ni doped ZnS NPs degrades the dye same as pristine ZnS, however, after 10 min a sudden fall of absorbance from 0.280 to 0.175a.u. is observed (Figure 4.12b).Almost 62% of the dye was degraded within the first 50 min. In case of 10 % Ni, the same amount of dye is degraded within first 20 min only and almost 70% dye degraded at the end of 80 mins (Figure 4.12c). The photo-degradation rates of RhB for all the samples are compared in Figure 4.S4.The plot of ln C_o/C vs irradiation time is a straight line and passes through the origin (Figure 4.S3 inset) indicates the first-order decay kinetics. The calculated rate constant (k) for pristine, 5 and 10% Ni doped ZnS

NPs are 0.00788, 0.0483, and 0.0548 min^{-1}, respectively. It is obvious from the results that photocatalytic degradation efficiency of ZnS NPs increases at 10% dopant level.

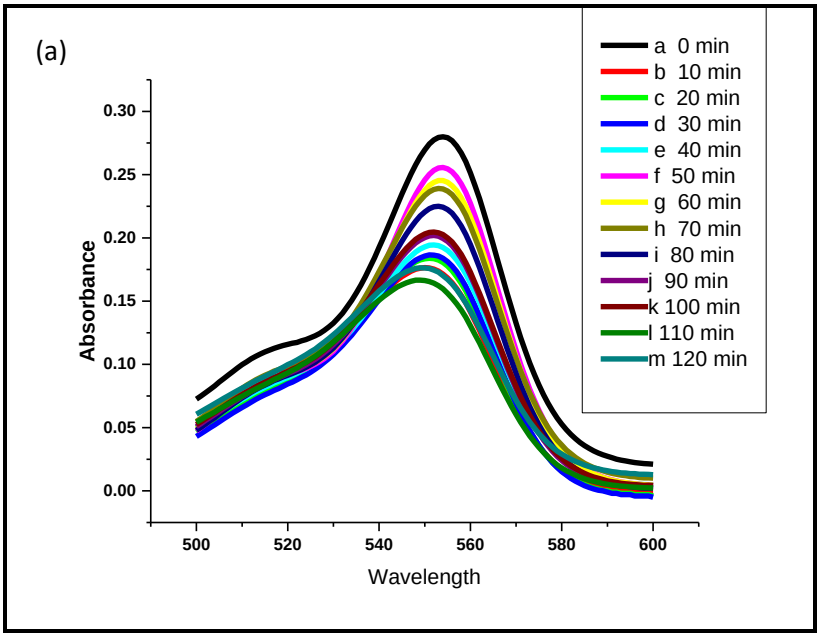

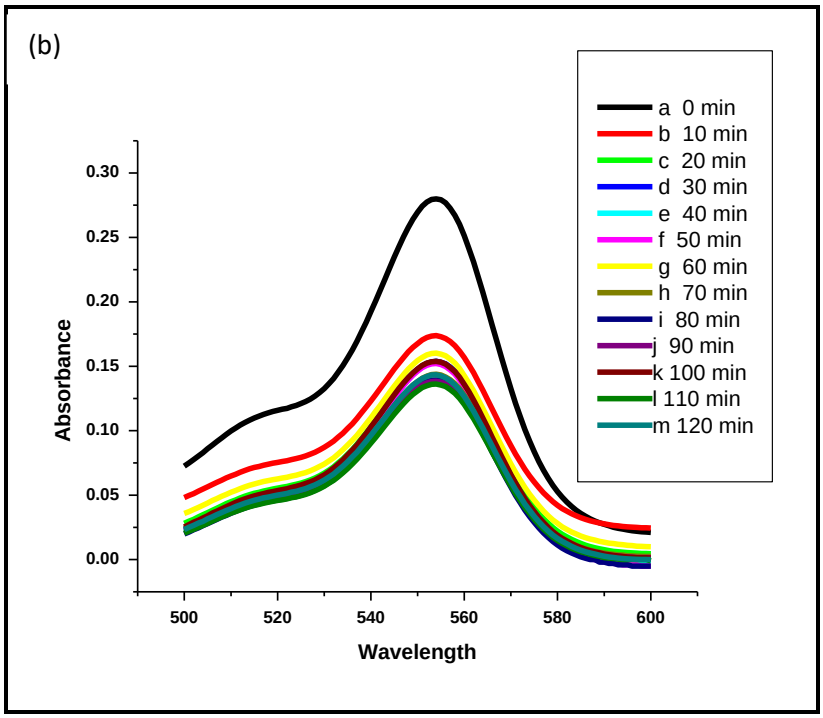

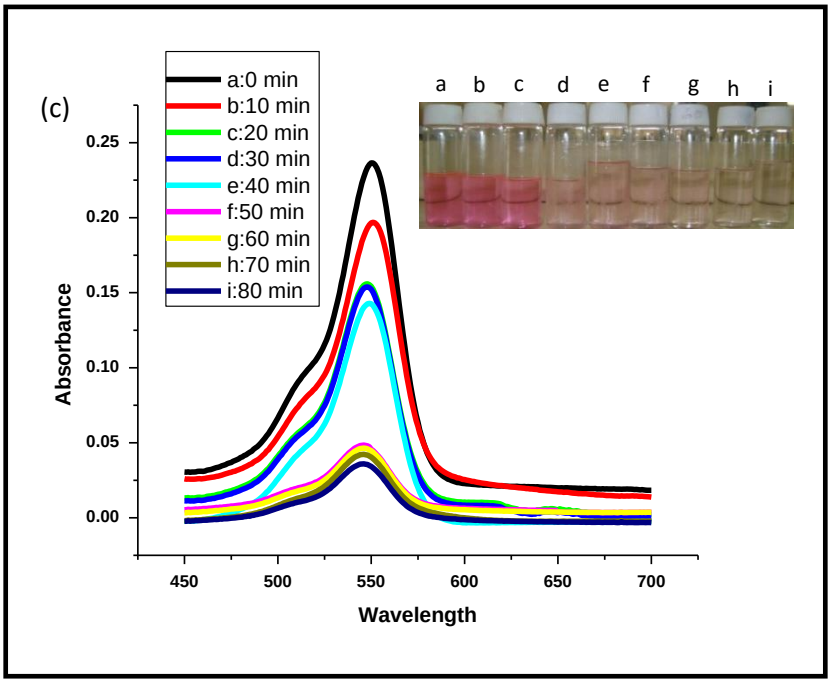

Figure 4.12.The photocatalytic degradation of RhB dye in presence of (a) pristine (b) 5% Ni^{2+} and (c) 10% Ni^{2+} doped ZnS NPs.

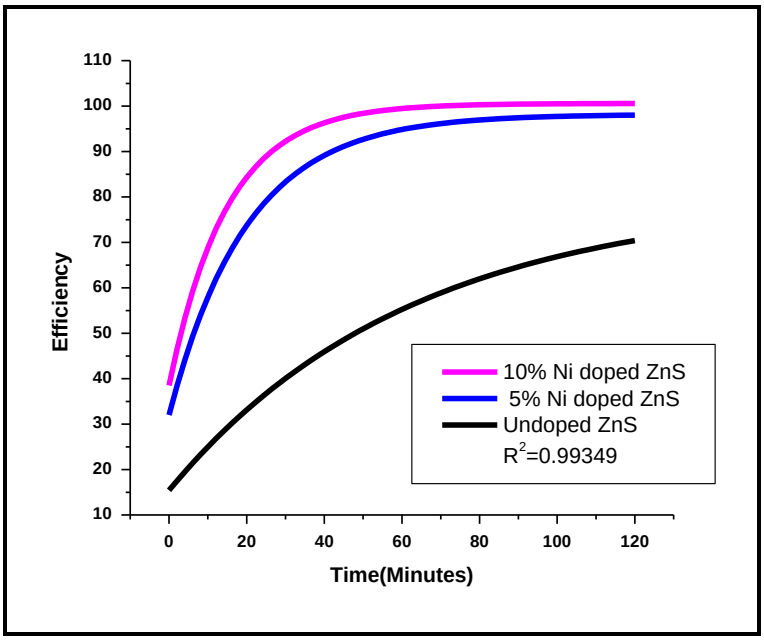

Figure 4.13.Comparison of the performance of pristine, 5 and 10% Ni doped ZnS NPs as photocatalyst for RhB dye with respect to irradiation time under HPMV lamp.

4.5 Mechanism of photocatalytic activity

Semiconductor nanoparticles act as light harvesting material. On exposure to light of wavelength equal to the band gap energy, the electrons present in VB excite to CB and produce h^+ and e^- in VB and CB of the host, respectively. These charge carriers should have sufficient life time to diffuse towards the surface and initiate oxidation/reduction reactions with the surface adsorbed reactant molecules before involving in the radiative and/or nonradiative recombination processes.[31, 33, 34]The role of dopant ions is important here: they provide extra energy levels and this wayreduce the band gap of the semiconductor and bring it to the visible or near UV

region, increase/decrease surface defects, increase the shallow or deep trap states, act as reaction sites for substrate molecules on the surface, etc. In the present work, it is observed from optical and kinetic studies that 10% Ni doped ZnS NPs show highest photocatalytic activity.Chauhan et al. evaluated the photocatalytic activity of Cu and Fe doped (3, 5 and 10 mol%) ZnS NPs using methylene blue dye. They concluded that 3 mol% of dopant concentration was required for the optimum performance of the catalyst[35, 36]. From these studies, it is proved that an optimum dopant concentration is required for better performance of the catalyst.[37] The present work shows that optimum performance is achieved at 10% Ni concentration (actual 5.24 wt% according to ICP-AES data) in ZnS NPs. The ability of a dopant to act as a trap site or to intervene the recombination of charge carriers depends on its location in the host (at substitutional or interstitial sites, on the surface or in the depth of the material), their actual amount in the host, particle size, etc. Figure 4.14 describes the mode of interaction of RhB with the surface of nanoparticles. Zn or Ni ions present on the surface may coordinate by vacant d orbital with electron-rich oxygen atoms or aromatic ring of RhB (by π bond-metal interaction). At nanoscale, the high surface to volume ratio increases the probability of a dopant to be present on the surface. This makes the interfacial diffusion of electrons and holes easier and thereby resulting in a faster reaction rate.[38]From the PL study, it is observed that at 10% dopant level, the lattice defects

decreases while the interstitial defects increases, which leads to more trapping of charge carriers.

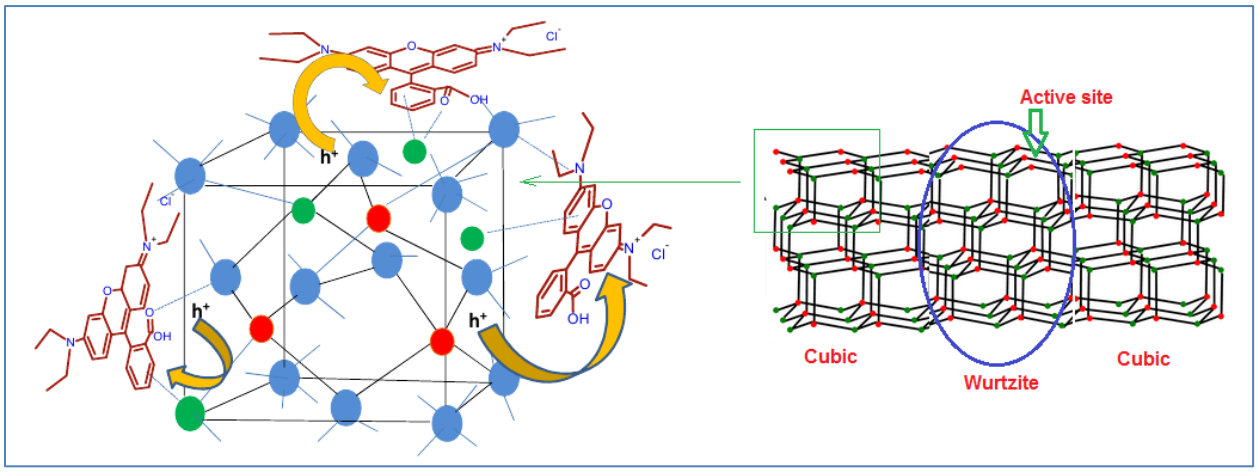

Figure 4.14.Surface interaction of Ni^{2+}doped cubic ZnS NPs with RhB dye molecules. The green, red, and blue balls represent Ni, Zn, and S ions, respectively.

To understand the effect of dopant ions on the Fermi level of the host semiconductor and in turn, mechanism of the photocatalytic activity, Mott-Sckottky (MS) measurements were carried out. For the purpose, the space-charge capacitance of the semiconductor surface was measured by varying the applied potential bias across the semiconductor in contact with electrolyte surface. Flat band potential was calculated from the plot of reciprocal of square of the space charge capacitance (C_{SC}) vs applied potential bias using the MS equation [39]

$$\frac{1}{{C_{SC}}^2} = \frac{2}{\varepsilon\varepsilon_0 N_d A^2}\left[(E - E_{FB}) - \frac{kT}{e_0}\right] + \frac{1}{{C_H}^2} \qquad (3)$$

where C_{SC} is the space charge capacitance of semiconductor, ε dielectric constant of ZnS, ε_0 the electric permittivity in vacuum, e_0 the elementary charge constant, N_d the donor density, A surface area, k Boltzmann constant, T the absolute temperature, E the electrode applied voltage, E_{fb} the flat band potential and $C_{H,}$ the Helmholtz (double layer) capacitance of electrolyte solution. Since the value of double layer capacitance is 2-3 orders of magnitude larger than the space charge capacitance, the contribution of $1/C_H^2$ term is negligible for the calculation of total capacitance. The donor density (N_d) was also calculated from the slope of the linear region using the equation[39]

$$N_d = -\left(\frac{2}{e_0 \varepsilon_0 \varepsilon}\right)\left(\frac{d(1/C^2)}{dE}\right)^{-1} \qquad (4)$$

It is known that MS analysis is valid under the charge carrier depletion condition within the semiconductor.[40, 41] In case of n-type semiconductor, depletion region arise (positive charges are dominant on the surface of semiconductor near the semiconductor-electrolyte interface) at potential bias positive of the flat band potential and vice versa for p-type. Due to charge depletion the band edges curve upward in case of n-type semiconductor and downward for p-type semiconductor. Intense electric field exists at the interface due to this. Hence, maximum separation of charge can be achieved on irradiation under this condition, which is favorable for photocatalytic activity. It can be observed from the Figure 4.15 that for each

sample under study, we kept the wide range of applied potential bias (-0.2 to 1.4 V vs SCE) such that transition from depletion to flat band condition can be achieved. It was observed that pH of the electrolyte solution can directly affect the measurement of $E_{fb.}$[42] Hence, NaH_2PO_4 buffer was used during the experiment to keep pH constant and 1M KCl was added as supporting electrolyte to increase the conductivity of the solution and maintain the potential difference across the interface. The positive slope of the line (linearly fit in the depletion region) for pristine and with 5% dopant confirm the n-type nature of the semiconductor. Flat band potential was calculated on extrapolating the straight line to X-axis ($1/C^2 = 0$) and donor density (in case of n-type) or acceptor density (in case of p-type) was calculated using equation 4. These values are tabulated in Table 4.1. If donor density calculated from this equation is considered as electron density (or negative charge density) then it can be seen that sufficient charge is available per unit volume of the pristine semiconductor surface to form depletion region and the Fermi level was established at -0.006 V (E_{fb}, vs NHE). Now, on doping 5% Ni in n-type semiconductor the donor density increases to an order of magnitude. This results into intensification of depletion layer and in turn, positive charge of semiconductor near the interface when keep in contact with electrolyte solution. So, the electrode acts as photoanode and does the oxidation of adsorbate. The higher value of E_{fb} (0.194 V vs NHE) in this case shows that more applied

potential bias is required to raise the depletion region to the Fermi level which would be equal to redox potential of the solution. On increasing the amount of dopant to 10%, it can be observed from the Figure 4.15 that the slope of the straight line becomes negative suggesting p-type nature of the semiconductor. This is also corroborated from the carrier density data (-1.70×10^{19} per cm^3) indicating acceptor (hole) density in semiconductor. This situation requires more potential bias, compared to previous case to achieve the Fermi level from depletion region.

The results of the MS analysis can be correlated with those of XRD. We proposed from XRD (and DSC analysis, Ref 21) analysis that at 0 and 5% dopant level, ZnS exists in Zinc Blende (ZB) phase in which majority of S^{-2} ions remain exposed on the front of the surface due to which a layer of negative charge is formed on the surface of semiconductor. Now when this type of semiconductor comes in contact with the electrolyte solution, movement of charge between semiconductor and solution takes place. In case of n-type, the electrons will be transferred from electrode into the solution and positive charge exists on the surface of electrode. Hence depletion region is generated in an open circuit condition which is a characteristic of n-type. On increasing the level of dopant to 10%, we proposed the presence of pockets of wurtzite (WZ) phase in which Zn^{2+} ions are present on the faces of crystal lattice and form the layer of positive Zn^{2+} ions at the surface near the interface. It is possible that high amount of WZ phase exists on the surface due

to high surface to volume ratio for NPs. When this semiconductor comes in contact with electrolyte solution, in an open circuit condition, positive holes are transferred to the solution and negatively charged electrons are exist on the surface of semiconductor and form the depletion layer, characteristic of p-type. These situations are picturized in Figure 4.16.

Table 4.1. Mott-Schottky parameters of synthesized ZnS NPs.

% Ni as dopant	**Slope x 10^{12}**	**Intercept x 10^{12}**	**Donor densities (N_d) cm^{-3} x 10^{19}**	**E_{fb} vs. SCE (vs. NHE) V**
0	1.460	1.35	1.09	-0.25 (-0.006)
5.0	0.817	1.02	1.94	-0.05 (0.194)
10.0	-0.933	2.13	-1.70	1.21 (1.454)

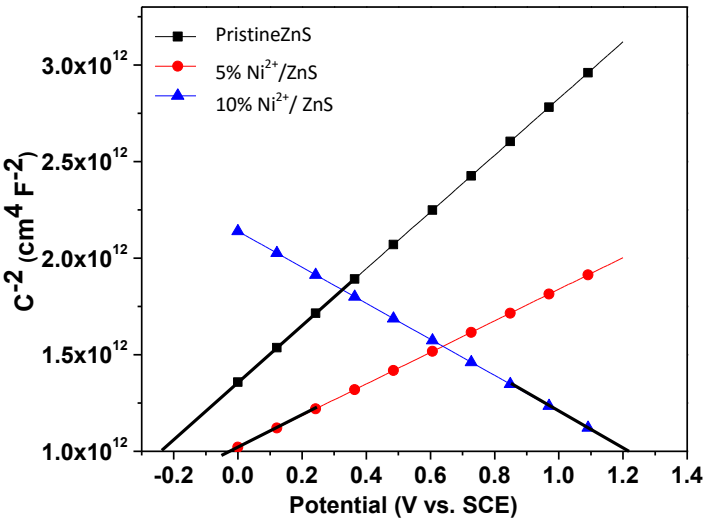

Figure 4.15.Normalized Mott–Schottky plot for pristine, 5.0 and 10% Ni^{2+} doped ZnS NPs.

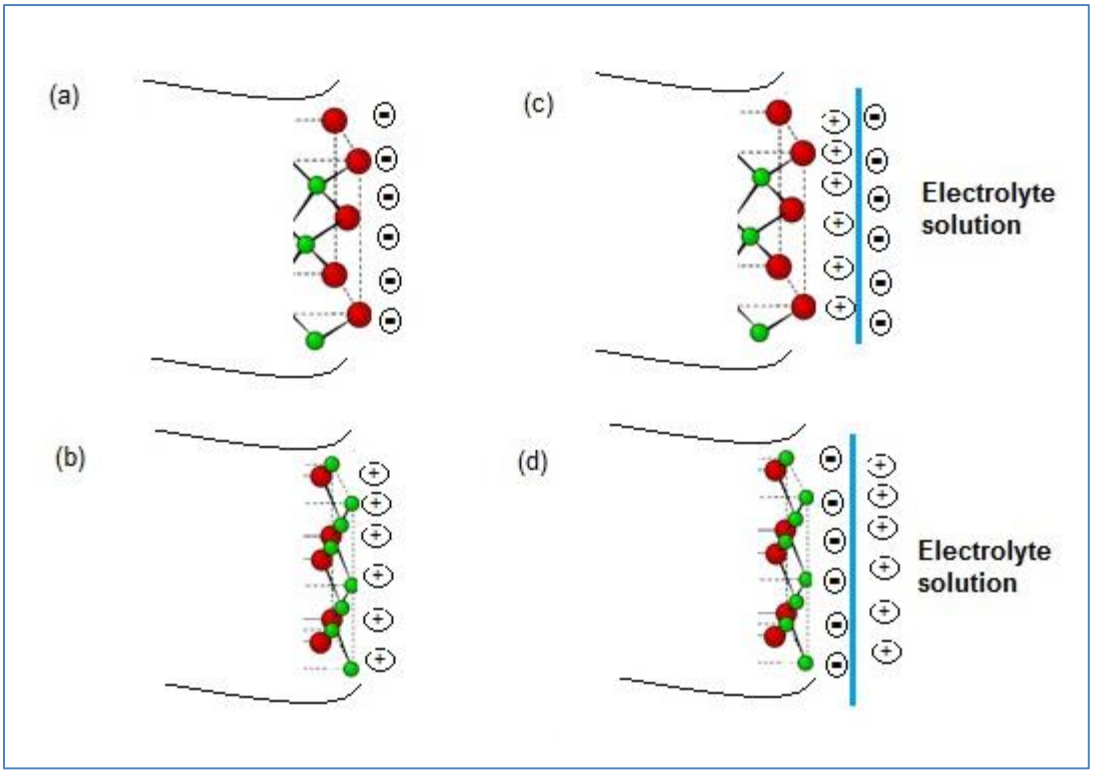

Figure 4.16.Schematic diagram of ZnS NPs as semiconductor electrode and its interaction with electrolyte solution. (a and c) electrode with ZB phase of ZnS NPs and electrode with ZB phase of ZnS NPs in contact with electrolyte solution having 0 and 5% dopant level (b and d) electrode with WZ phase of ZnS NPs and electrode with WZ phase of ZnS NPs in contact with electrolyte solution.

Cyclic voltammograms of the ZnS (with and without doping) NPs as working electrode are shown in Figure 4.17. It is noted that pure ZnS NPs electrode exhibit cathodic current under negative applied potential. In dark, the negative potential, compared with the flat band potential, generates an accumulation layer and as a result the electrode of ZnS can act as a (dark) cathode that can reduce oxidized species of solution. This behaviour confirms the *n*-type character of pristine ZnS NPs. [43]As the Ni^{2+} doping increases, along with cathodic current at negative potential, an additional peak with anodic current at positive applied potential is observed (for 10% Ni in ZnS NPs). The higher anodic current and the lower cathodic current, signify that 10% or higher doping with Ni^{2+}decrease the *n*-type conductivity and increase the *p*-type conductivity of semiconductor. Hence, the surface adsorbed dye molecules encounter large number of holes on the surface due to high surface to volume ratio in nano regime.

In order to confirm the nature of semiconductor observed in CV analysis, hot-probe analysis was carried out. [44] The semiconductor shows positive potential at the hot-probe terminal for *n*-type while reverse is true for *p*-type (Table 4.2). The analysis shows that pristine ZnS and 5% Ni doped ZnS NPs are of *n*-type semiconductors while 10% Ni doped ZnS NPs of *p*-type, in agreement with the CV data.

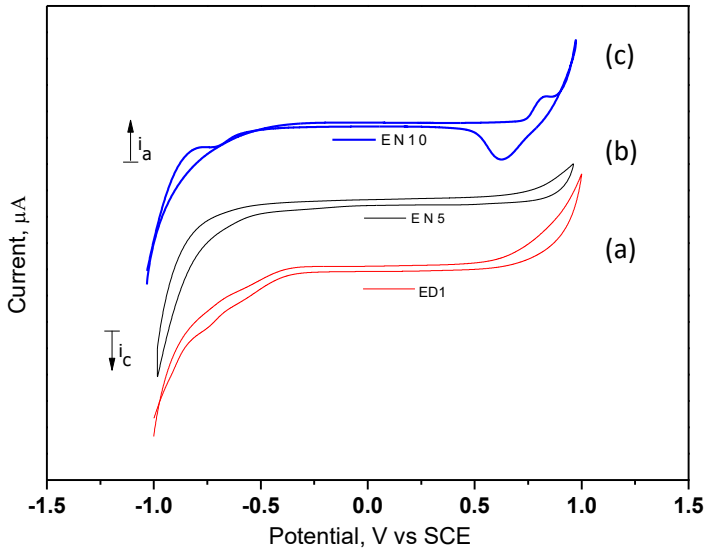

Figure 4.17.Cyclic Voltammogram of (a) pristine (b) 5%Ni^{2+} and (c) 10% Ni^{2+}doped ZnS NPs as a working electrode in aqueous solution.

Table 4.2. Evaluation of semiconductor type by hot-probe measurements.

Sr.No.	Sample	Voltage (V)
1	ZnS (pristine)	+0.37[a]
2	ZnS/Ni^{2+} 5%	+0.26[a]
3	ZnS/Ni^{2+} 10%	-0.24[b]

a: positive potential for n-type semiconductor and ***b*:** negative potential for p-type semiconductor

This may be due to filling of S^{2-} vacancies by Ni^{2+} ions that decreases the availability of electrons in ZnS NPs.[45]At 10% dopant level, the excess Ni^{2+} ions collected more on the surfaces either at interstitial vacancies or remain adsorbed at

residual valances due to the high surface-to-volume ratio, thereby providing sites for dye molecules to be adsorbed on the surface. Further, we could correlate this observation with that of our previous study where we reported that at 10% dopant concentration, phase change is observed in the material due to lattice strain. We proposed the presence of 'local pockets' of wurtzite phase within the overall cubic phase of host matrix. These local pockets may also provide sites for the adsorption of the dye molecules. We could not increase the amount of dopant ions more than 10% (5.72% actual) by the experimental method reported in this study. This study should be considered as a model, Ni^{2+} may not be able to reduce the band gap and bring it to the visible region. However, this can be done by changing the dopant ions. Hence, these observations invite further research in this area.

4.6. Conclusion

ZnS NPs (pristine and doped with 5 and 10% Ni^{2+}) were synthesized by simple wet chemical method. The XRD patterns suggest that the crystallinity increases on increasing the amount of dopant due to a decrease in lattice defects. At 10% dopant concentration, the intensity of PL at 425 nm is diminished and that of at 330 nm increases compared to pristine NPs due to trapping of charge carriers at shallow trap states indicating enhancement of photocatalytic efficiency. The actual amount of dopant and their location in the material are factors that govern the photocatalytic performance. The dopant ions play a role to (1) alter the band gap

(2) shift the nature of semiconductor from n to p-type (3) coordinate with organic reactants on the surface and (4) induce phase change in a material,synergistically enhance the degradation efficiency of the catalyst. The present study shows that the character (n/p type) of the semiconductor is an important parameter affecting the photocatalytic activity. At 10% dopant level, the material converts into p-type and becomes capable of oxidizing the adsorbed dye pollutants. Practically, such type of tailored materials can be deposited on inert and robust surfaces and on exposure to light can be used to treat polluted water effectively.

References

(1) N. Serpone ; A. V. Emeline, *J. Phys. Chem. Lett.*2012, **673** ,3.

(2) S.C. Ke;T., T.C.Wang, M.S.Wong and N.O. Gopal, *J. Phys. Chem. B* 2006, **11628** ,110.

(3) E. A.Weiss , *Acc. Chem. Res.* 2013, **2607** , 46.

(4) J. Zhang, J. Yu, Y. Zhang, Q. Li and J.R. Gong, *Nano Lett.*2011, **4774** ,11.

(5) A.P.Alivisatos ,*Science* ,1996,, **933** ,271.

(6) L. E.Brus, *J. Chem. Phys.*1984, **4403**,80.

(7) Y. S. Wang, P.J. Thomas and P.O. Brien, P. O., *J. Phy. Chem. B* 2006, **21412**,110.

(8) H. Chander, *Mater. Sci. Engg. R* 2005, **113**,49.

(9) H.Libiadh, T.B. Chaabane, L. Balan, N. Becheik, S.Corbel, G.Medjahdi and R. Schneider, *Appl. Catal., B* 2014, **29** ,144.

(10) S. Li, L. Zhang, T. Jiang, L. Chen, Y. Lin, D. Wang and T.Xie, *Chem. Eur. J.* 2014, **311**,20..

(11) X. Zong, H. Yan, G. Wu, G. Ma, F. Wen, L. Wang, and C. Li, *J. Am. Chem. Soc.*2008, **7176**,130.

(12) M. Radoičic´, Z. Šaponjic´, I. A. Jankovic´, G. Ćiric´-Marjanovic´, S. P.Ahrenkielc and M. I. Čomora, *Appl. Catal., B* 2013, ***136,* 133.**

(13) W.P.Wuelfing, S.J. Green, J.J. Pietron, D. E. Cliffel, R. W. Murray, *J. Am.Chem. Soc.*2000, **11465**,122.

(14) G.Xi, C. Wang, X.Wang, Q. Zhang and H. Xiao, *J. Phys. Chem. C* 2008, **1946**,112.

(15) B. Y.Geng, X.W. Liu,Q.B. Du, X.W. Wei and L. D. Zhang, *Appl. Phys. Lett.*2006, **163104**,88.

(16) J. Zhuang, X. Zhang, G. Wang, D. Li, W.Yang and T. Li, *J. Mater. Chem.* 2003, **1853**,13.

(17) R. N.Bhargava, *J. Lumin.*1996, **85,**70.

(18) H.R.Pouretedal, A. Norozi, M.H. Keshavarz and A.J.Semnani, *J. Hazard. Mater.*2009,**674**, *162*.

(19) J. H. Bang, R.J. Helmich and K.S. Suslick , *Adv. Mater.*2008, *20*, **2599**,20.

(20) Y.Chen, R.H.Yin and Q.S. Wu, *J. Nanomater.*2012, **1**, DOI: 10.1155/2012/560310.

(21) .N. Dixit, N. Anasane, M. Chavda, D. Bodas and H.P.Soni,*Mater. Res. Bull.*2013, **2259**,48.

(22) The spectrum from HPMV light and its comparison with natural light is available at

http://www.lamptech.co.uk/Documents/Datasheets/DS%20Westinghouse%20Mercury%201950.pdf.

(23)X.Yu, J. Yu and B. Cheng, Huang, B.,*Chem. Eur. J.*,2009, **6731**,15.

(24)R. Jenkins and R.L. Snyder, Introduction to X-ray powder diffractometry. NewYork: John Wiley and sons, **1996**.

(25) N. Dixit, H.P. Soni, *SuperlatticesMicrostruct*.2014, **344**,65.

(26) R. Rossetti, R. Hull, J.M.Gibson and L.E. Brus, L. E., *J. Chem. Phys.*1985, **552**,82.

(27) D. E.Dustan, A. Hagfeldt, M. Almgren, H.O.G. Siegbahn and E.Mukhtar, *J. Phys. Chem.*1990, **6797** 94.

(28) J.Tauc, R. Grigorovici and A.Vanuc, *Phys. Status Solidi* 1966, **627,**15.

(29) A. Kudo and M. Sekizawa, *Chem. Commun*.2000, **1371**.

(30) A. Goudarzi, G.M. Aval, S.S. Park, M.C. Choi, R. Sahraei, M.H.Vallah, A. Avane, Ha, *Chem. Mater*.2009, **2375**,21.

(31) S. Lee, D. Song, D. Kim, J. Lee, S. Kim, I.Y. Park and Y.D. Choi, *Mater. Lett.*2004, **342**, 58.

(32) Kudo, ,*Pure Appl. Chem.*2007, **1917**,79.

(33) D.Zhang, G. Li, H. Li and Y. Lu, *Chem. Asian J*.2013, **26**,8.

(34) J.Yang, D. Wang, H. Hau and C. Li, *Acc. Chem. Res.*2013, **1900**,46.

(35) R. Chauhan, A. Kumar and R. P.Chaudhary, *J. Lumin.*2014, **6** ,145.

(36) R. Chauhan, A. Kumar and R.P. Chaudhary, *Spectrochim. Acta.A* 2013, **250** , 113.

(37) W. Choi, A. Termin and M.R. Hoffmann, *J. Phys. Chem.* 1994, **13669**,98.

(38) Q. Xiao, Z. Si, J. Zhang, C. Xiao and X. Tan,,*J. Hazard. Mater*.2008, **62 ,**150

(39) W.D.Zhang, L.C. Jiang and J.S. Ye, *J. Phys. Chem. C* 2009, **16247**,113.

(40) A. Bott, Curr. Separations 1998, **87**,17.

(41) G. Natu, P. Hasin, Z. Huang, M.Ji, Y. He and Y.Wu, *ACS Appl. Mater. Interfaces* 2012, **5922**,4.

(42) H. Gerischer, Electrochim. *Acta* 1989, **1005**,34.

(43) A. J. Bard and L.R. Faulkner, *Wiley-India*, **2004,** pp. 752, Ch. 7.

(44) G. Golan, A. Axelevitch, B. Gorenstein and Manevych, *Microelectron. J.***2006**, **910**, 37.

(45)J.C. Wu, J. Zheng, P. Wu and R. Xu, *J. Phys. Chem. C* 2011, **5675 ,**115.

Table 4.S1: Percentage Ni (atomic wt%) as dopant in ZnS host determined by ICP-AES.

Sr. No.	Amount of Ni taken	Ni/Zn (at%) determine by ICP-AES	Ni (wt%) determine by ICP-AES	Zn (wt%) determine by ICP-AES	Band gap energy (eV)
1	0	-	-	-	4.43
2	5.0	6.24	2.82	45.24	4.28
3	10.0	10.28	5.24	50.93	4.29

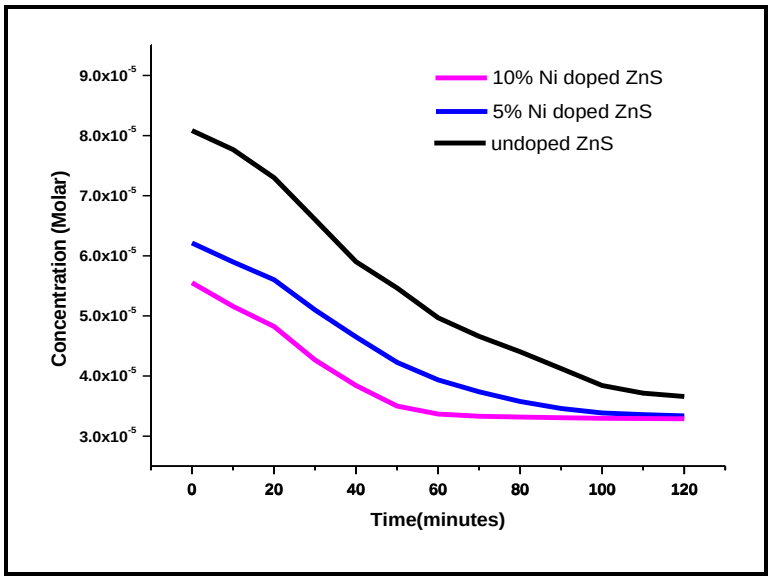

Figure 4.S1. Change in concentration of RhB with time in presence of pristineZnS nanoparticles and ZnS nanoparticles doped with 5 % and 10 % Ni^{2+}.

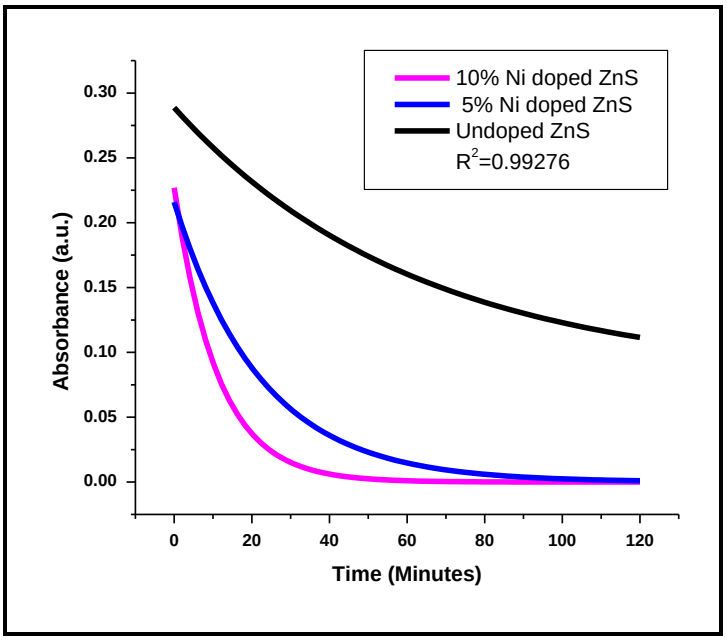

Figure 4.S2. Decomposition of RhB with time in the presence of pristine ZnS nanoparticles and ZnS nanoparticles doped with 5% and 10% Ni^{2+}.

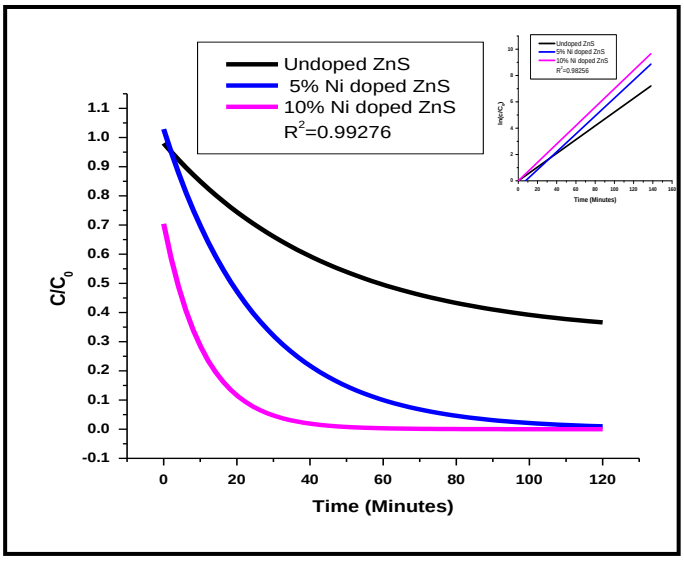

Figure 4.S3.Photodegradation of RhB in presence of pristine, 5and 10% Ni^{2+} doped ZnS NPs (inset shows ln C_o/C vs. time plot).